Nuclear Instruments and Methods in Physics Research B 557 (2024) 165544

Contents lists available at ScienceDirect

Nuclear Inst. and Methods in Physics Research, B

journal homepage: www.elsevier.com/locate/nimb

Full Length Article

Minimum detectable levels of biologically relevant elements in P8 filter paper standard using PIXE spectroscopy

Charles T. Bowen, Todd A. Byers, Cory Nook, Darshpreet Kaur Saini, Bibhudutta Rout *, Gary A. Glass *

Ion Beam Laboratory, Department of Physics, University of North Texas, Denton, TX, USA

ARTICLE INFO

Keywords:
PIXE
Minimum detectable level
Trace element
X-ray

ABSTRACT

PIXE analysis was conducted on p8 fisher brand filter paper samples soaked in elemental standard solutions to determine the minimum detectable levels of Al, Si, P, S, Cl, K, Ca, Cr, Fe, Ni, Cu, and Se. All samples were analyzed with beam parameters of 2 μC incident charge, and beam current of less than 2 nA at 2 MeV beam energy. Minimum detectable levels were obtained by analyzing the x-ray spectrum in the GeoPIXE analysis package, and the data for each element would be averaged over all collected spectra. The minimum detectable level in parts per million was found to be on average 9.59 for Al, 4.6 for Si, 3.23 for P, 2.27 for S, 1.82 for Cl, 1.15 for K, 0.88 for Ca, 0.51 for Cr, 0.07 for Mn, 0.54 for Fe, 1.59 for Ni, 2.0 for Zn, 1.55 for Cu, and 6.5 for Se. Minimal deviation from the averaged values was observed, except in cases where samples contained high concentrations of elements with overlapping X-ray energies.

1. Introduction

A large body of evidence points to the key role that trace amounts of fourth period metallic elements play in regulating biological functions. In trace amounts, metals such as Fe, Cu, Co, Mg and Mn play an essential role in ensuring proper brain function and growth. In excess amounts these same trace elements are associated with several adverse neurological diseases like Parkinson's, Alzheimer's disease, and Wilson's disease [1–5]. Similarly, Zn plays a key role in several biological processes, including neurotransmission and modulating the activity of various proteins, but it may also cause apoptotic cell death in deficient organisms [6,7]. Absorption of toxic heavy metals and monitoring the uptake of essential trace elements into crops is also another topic of concern [8,9]. There is even some evidence to suggest that ultra-trace elements (at concentrations of ng/g or less) such as F, Pb and V are essential to proper growth and brain function [10]. Because of this, there is a critical need to understand the concentration and transport of metallic trace ions in tissue. A previous analysis of rat brain tissue samples has determined that the concentration of metallic trace elements in brain tissue is on the order of parts per million (PPM) to parts per billion (PPB) [11]. Due to its great sensitivity on the order of ~1 ppm, particle induced X-ray emission spectroscopy (PIXE) is an excellent analytical tool for studying the concentration of these trace elements in biological tissues [12,13]. Other techniques like scanning electron microscopy (SEM) or secondary ion mass spectrometry (SIMS) are typically limited in their ability to quantify the concentration elements in a sample. Additionally, these same techniques may damage or destroy parts of the sample in the process depending on experimental conditions. Micro-PIXE analysis allows for nondestructive quantitative analysis of trace elements at a cellular or sub-cellular level [14]. Due to this nondestructive nature, other analytical ion beam techniques like particle induced gamma ray spectrometry (PIGE), Rutherford backscattering spectrometry (RBS) and nuclear reaction analysis (NRA) can also be run simultaneously while acquiring data using PIXE. This provides useful information about the depth distribution of elements within the sample along with the concentration of lighter elements in the matrix. Many studies have been conducted using this for trace element analysis, especially when it comes to monitoring the distributions of trace elements in biological tissue, aerosol samples, archeology and geology [15–17]. Given PIXE techniques suitability for biological analysis, determining the minimum detectable level (MDL) of these trace elements is of great interest, especially in biological applications. Since the continuous X-ray background produced by a sample is highly dependent on the sample composition [18], easily preparable standards with similar composition to the sample of interest is needed to test system limits. Previous studies have investigated the use of photoengraving glue

* Corresponding authors.
E-mail addresses: bibhu@unt.edu (B. Rout), Gary.Glass@unt.edu (G.A. Glass).

https://doi.org/10.1016/j.nimb.2024.165544
Received 4 February 2024; Received in revised form 16 August 2024; Accepted 13 October 2024

Table 1
Order of soaked elemental standards for Fe-Cu-Se mixture samples.

Sample	1st solution	2nd solution	3rd solution
Fe-Se-Cu	Fe	Se	Cu
Se-Cu-Fe	Se	Cu	Fe
Cu-Fe-Se	Cu	Fe	Se

for preparing known elemental standards simulating biological tissue, while others have used pure gold targets to simulate archeological samples [19,20]. Fisher Scientific p8 filter paper [21], being readily available and comprised mostly of cellulose $(C_6H_{10}O_5)_n$, also serves as a potential candidate for simulating biological matrices. This paper investigates several biologically relevant trace elements present in brain tissue, including S, P, K, Ca, Mn, Ni, Zn, Fe, Cu and Se, and their associated MDL in a simulated biological matrix.

2. Sample preparation and methods

2.1. Single element sample preparation

Samples were prepared by cutting out a 1″ diameter disk out of Fisher Scientific P8 filter paper with a dry thickness of approximately 180–200 μm. Individual prepared samples were then placed into a glass petri dish and 3 to 5 drops of approximately 0.05 ml per drop of an NIST certified elemental standard solution were dropped directly onto the paper, until the filter paper was soaking in a small pool of the absorption standard. This was to ensure that the atomic absorption standard would completely saturate the filter paper and ensure an even distribution of the elemental standard solution. The samples would be left to soak in the elemental standard of interest for approximately 2 min, after which they would be placed on a sheet of aluminum foil and left to dry for approximately 24 h. After the samples finished drying, they were weighed, and the areal density could be obtained by taking the ratio of the sample's mass to its area. Combined with the listed volume density of the manufacturer (0.10–0.15 g/cm^3), this allows for the determination of the thickness of each sample. On average samples were found to have an average thickness of 198.29 μm. Each sample was then cut in half, and two samples were affixed to a single 1″ diameter aluminum ring using double sided carbon tape. The rings were secured in a sample holder and mounted to the stage prior to analysis.

2.2. Multiple element sample preparation

Several samples were made with a combination of different elemental standard solutions to test multiple variables. The main objective was to evaluate whether the MDL of elements changed when an increased concentration of other elements was present. Additionally, samples containing elements that have overlapping K_α and K_β X-ray energies were made to determine if high X-ray overlap had an impact on the MDL. Samples doped with multiple elements were made using a similar method detailed earlier. Elemental standard solutions would be directly deposited onto a filter paper matrix and be left to soak for 2 min. The sample was then immediately transferred to a new dish, and the process would be repeated with a new standard solution until it had been doped with all desired elements. Completed samples were then dried, weighed and mounted to the sample holder as described in the previous section. Three different samples were made using a mixture of Fe, Cu and Se solutions to test whether the order in which the solutions were soaked affected how much of each solution the sample absorbed. Table 1 shows the solution order in which the three Fe-Se-Cu combination samples were soaked. Finally, a single sample was prepared by marking filter paper directly with a marker pen to obtain a contaminated spectrum. In total, 10 single element samples, 9 combination element samples, and two control/contaminant samples were analyzed.

2.3. Experimental setup

The experimental setup of the beam chamber is schematically shown in Fig. 1 and has been previously described in detail in papers done by Rout et al. [22–24]. A 2 MeV proton beam was produced by an NEC 3 MV 9 SH single ended Pelletron accelerator. X-ray data was acquired using an Amptek X-123 Fast SDD detector equipped with a C1 window [25] with an approximate solid angle of 42.5 msr. An Ortec 142A preamplifier with an Ortec 671 amplifier with a 1 μs pulse shaping time was used to collect the electronic signal. A Canberra 8701 ADC was connected to the Oxford Microbeams data acquisition (OMDAQ) system. Beam size was chosen to be 1 × 1 mm^2, and beam current was maintained at less than 2 nA to ensure minimal damage to the samples. An optical camera was used to position the samples and data was collected using OMDAQ software. Collected X-ray data was analyzed using the GeoPIXE software package.

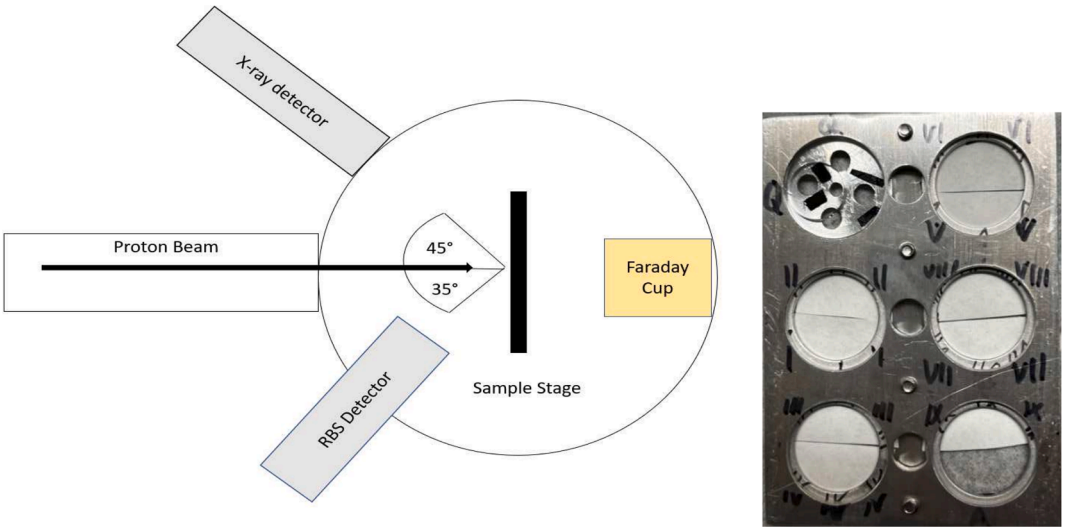

Fig. 1. Schematic diagram of the irradiation chamber and samples mounted on the stage adaptor, showing direction of beam travel and approximate locations of detector systems.

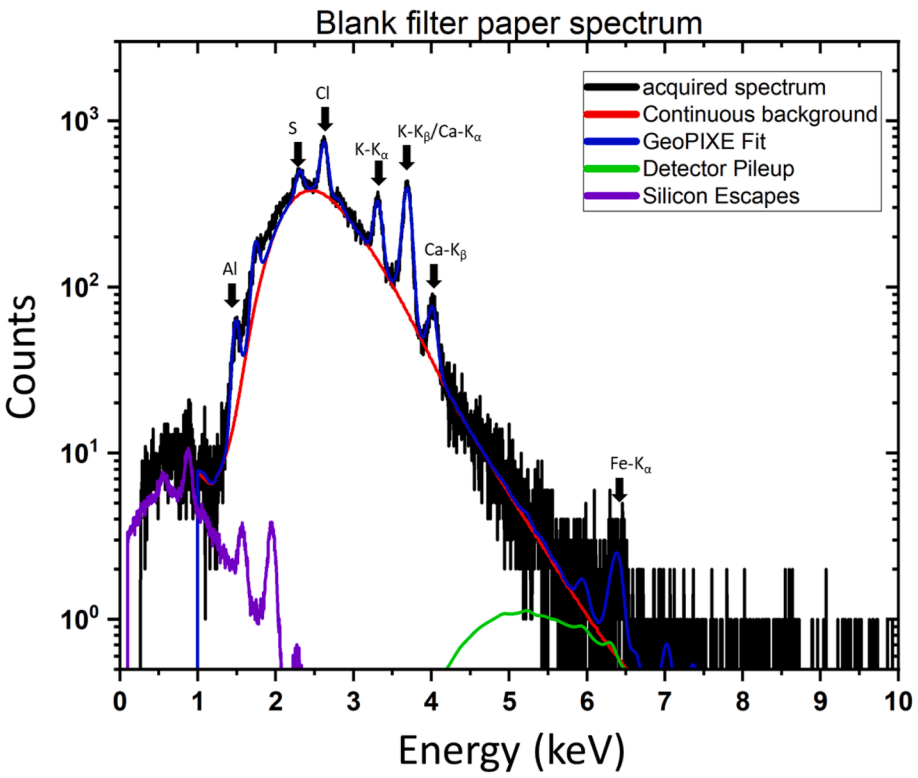

Fig. 2. PIXE spectrum for an undoped piece of p8 fisher scientific filter paper. With background components and GeoPIXE line of best fit overlaid onto the spectrum.

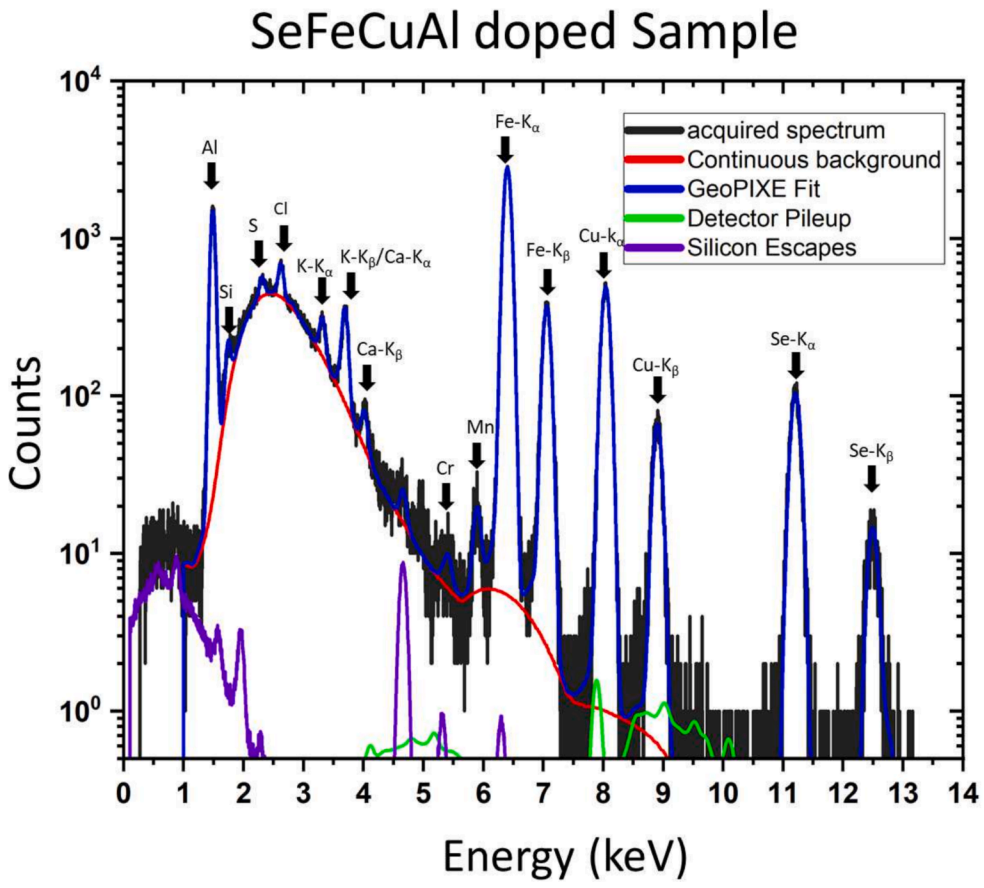

Fig. 3. PIXE spectrum for the Se-Fe-Cu-Al doped p8 fisher scientific filter paper with aluminum contamination present, with background components and GeoPIXE line of best fit overlaid onto the spectrum.

Table 2
MDL for elements in each prepared sample doped with a singular elemental solution.

Solution deposited onto filter paper	MDL of elements (PPM)									
	P	S	K	Ca	Mn	Fe	Ni	Cu	Zn	Se
None/blank	–	2.2	1.1	0.87	–	0.42	–	–	–	–
P	3.4	2.3	1.2	0.88	–	0.39	–	–	–	–
S	–	2.3	1.1	0.87	–	0.038	–	–	–	–
K	–	2.1	1.1	0.87	–	0.4	–	–	–	–
Ca	–	2.1	1.1	0.89	–	0.37	–	–	–	–
Mn	–	2.4	1.2	0.93	0.73	0.99	–	1.3	–	–
Fe	–	2.2	1.1	0.82	–	0.73	–	–	–	–
Ni	–	2.3	1.1	0.87	–	0.5	1.7	–	–	–
Cu	–	2.1	1	0.79	–	0.39	–	1.7	–	–
Zn	–	2.5	1.3	0.98	–	0.44	0.98	1.4	2.2	–
Se	3	2.1	1.2	0.96	–	0.45			–	6.9
Standard Deviation	0.283	0.129	0.078	0.052	–	0.183	0.509	0.208	–	–
Average MDL:	3.22	2.23	1.14	0.884	0.73	0.496	1.34	1.46	2.2	6.9

3. Results and discussion

3.1. PIXE background components and MDL

PIXE Spectra are subject to both a continuous and discrete background stemming from both physical and electronic processes. The main components that contribute to the continuous background of a PIXE spectrum are secondary electron bremsstrahlung (SEB), and proton bremsstrahlung [13]. Figs. 2 and 3 display typical PIXE spectra of an undoped piece of filter paper and a doped piece of filter paper respectively, along with the different background components present.

As high energy protons traverse through a target, they will lose energy by ionizing atoms they encounter, ejecting electrons from their respective atomic shells. Ejected electrons will be slowed by coulombic interactions with other atoms in the sample and will emit SEB. The SEB is the major component of the portion of the continuous background that is below the maximum energy that can be transferred from an incident proton to an atomic electron [13]. Protons will also emit bremsstrahlung as they are slowed by interactions with target nuclei. This proton bremsstrahlung contributes to the continuous background as well. However, it decreases with energy and is typically insignificant in the low energy region where the SEB background is dominant. Along with the continuous background, a series of discrete background components are present, and stem from the electronic equipment used during experimentation. Detector pileup occurs when two or more detectable events interact with the x-ray detector before the voltage signal from a single event can be swept out of the detector. This results in a counting error, and results in the incident signals being registered as a single event with a combined total energy. Another discrete background component that is often present in PIXE spectra are silicon escape peaks. These occur when a silicon atom inside of the detector crystal is ionized due to the interaction of the incoming photons with the detector material. This results in the emission of a silicon x-ray (typically a Si-k_α x-ray of 1.74 keV). Should the Silicon x-ray escape the detector volume, the x-ray detector will register an artificial peak with an energy of 1.74 keV minus the original energy of the x-ray that entered the detector. To determine the MDL of an element in a sample, the x-ray signal produced by the element must be distinguishable from the background present at that energy level. The MDL then is the minimum concentration of an element that must be present within a sample, for the x-ray peak that is produced to be distinguishable from the background. Because of this, the MDL of any element is heavily dependent on its matrix composition, as different matrices will yield different background spectrums. MDLs are also heavily dependent on beam energy, however for elements with atomic numbers between 20–30, the beam energy which yields the lowest MDL is typically between 1–2 MeV. It is customary practice to define the detection limit of an element, as the concentration required to give rise to a net x-ray peak intensity of at least 3 times the standard deviation of the background intensity: [13].

3.2. GeoPIXE fitting

After the x-ray emission data for each sample was collected, the spectra data was imported into the GeoPIXE analysis package, and analysis was carried out in the thick target approximation, using the areal density of each sample and the known volume density of cellulose of 1.5 g/cm^3. Information about the experimental setup such as charge incident on the sample, beam current, filter paper composition, areal density of the sample, volume density, detector geometry, and detector type were all input into the program. This information is used by GeoPIXE to calculate the x-ray yield of the sample matrix, detector pileup, silicon escape peaks, and solid angle of the detector. This allows

Table 3
MDL for elements in each prepared sample doped with multiple elemental solutions.

Solution(s) deposited onto filter paper	MDL of elements (PPM)									
	P	S	K	Ca	Mn	Fe	Ni	Cu	Zn	Se
Se-Cu-Fe	–	2.4	1.2	0.91	–	0.65	–	1.4	–	6.5
Fe-Se-Cu	–	2.3	1.2	0.93	–	0.44	–	1.5	–	6.9
Cu-Fe-Se	–	2.4	1.2	0.9	–	0.54	–	1.4	–	6.6
Cu-Se	–	2.4	1.2	0.9	–	0.44	–	–	–	6.8
Fe-Se	–	2.3	1.2	0.87	–	0.59	–	1.6	–	6.5
Fe-Cu	–	2.4	1.2	0.91	–	0.71	–	1.4	–	6.7
Fe-Cu-Se-Al	–	1.9	0.96	0.73	0.73	0.72	1.7	1.1	–	5.1
P-Ca	3.1	2.2	1.1	0.87	–	0.39	–	1.4	–	–
Ni-Cu	3.4	2.5	1.2	0.93	–	0.55	2.1	2.9	2.2	–
Standard Deviation	0.21	0.17	0.08	0.06	–	0.13	–	0.55	–	0.61
Average MDL:	3.25	2.31	1.16	0.89	0.73	0.56	2.1	1.59	1.8	6.44

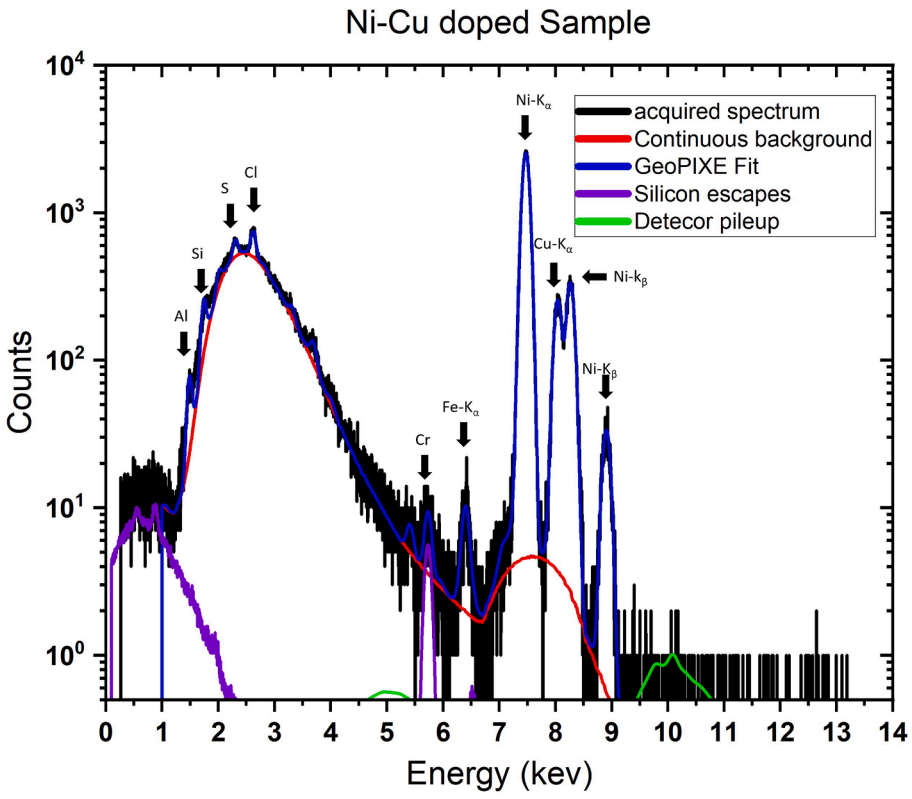

Fig. 4. A typical x-ray spectrum fit using GeoPIXE for the Nickel and Copper combination doped sample. Violet line represents silicon escape peaks, blue line is a line of best fit, and green is x-ray detector pileup. The overlapping peaks of the Nickel K-β and Copper K-α result in difficult to interpret spectrum. (For interpretation of the references to colour in this figure legend, the reader is referred to the web version of this article.)

GeoPIXE to simulate the x-ray background and identify trace elements not normally present in the sample matrix. GeoPIXE allows users to input trace elements that are thought to be present in the sample to generate the best fit for the sample spectrum. This fit is generated using spectral decomposition transformation that closely approximates a reduced Chi-squared model. The program then relates the area of the deconvoluted x-ray peaks to the concentration of trace elements present within the sample [26]. A detailed explanation of which can be found in the GeoPIXE user manual, and in papers written by Ryan et al. [27,28]. When a sample's spectrum was loaded into the program, elements within the sample would be identified by observing the distinguishable characteristic x-ray peaks present. These elements would then be input into the fitting program. After all suspected elements were input into the program and a fit was generated, information such as fitting parameters, detection limits, uncertainty, concentration, and MDL of each element present within a sample could then be exported as a CSV file for further analysis.

Table 4
MDL of elements not originally intended for study in all prepared samples.

Solution(s) deposited onto sample	MDL of elements (PPM)			
	Al	Si	Cl	Cr
none	8.8	4.3	1.8	–
P	10	4.9	1.9	–
S	10	4	1.8	–
K	9.6	4.4	1.7	–
Ca	9.2	4.5	1.7	0.4
Mn	10	4.8	2	0.75
Fe	8.7	4.4	1.7	0.48
Ni	9.3	4.6	1.8	–
Cu	8.6	4.1	1.6	0.39
Zn	10	5	2	–
Se	11	4.6	1.8	–
SeCuFe	10	5	1.9	–
FeSeCu	9.5	4.6	1.9	–
CuFeSe	9.3	4.7	1.9	–
CuSe	9.9	4.9	1.9	–
FeSe	9.4	4.8	1.9	–
FeCu	9.4	4.6	1.9	0.52
FeCuSeAl	9.2	4.2	1.5	0.45
PCa	9.7	4.6	1.7	0.41
NiCu	9.9	4.8	2	0.52
Standard deviation	0.562	0.276	0.132	0.055
Average MDL	9.565	4.595	1.82	0.884

3.3. PIXE analysis of prepared samples

Table 2 lists the MDL for elements present in each prepared sample generated using the GeoPIXE software. MDL's were automatically determined based off the combined statistics of both the K_α and K_β peaks when applicable.

Despite the concentrations of elements present varying dramatically between blank and prepared samples, the MDL for every element remains relatively constant throughout each sample. This indicates that the MDL for each element is independent of the concentration of the element present, which is to be expected. As mentioned previously, several samples containing multiple different elemental mixtures were analyzed to determine the effect on the MDL of each element.

Table 3 Lists the elemental combinations used, and the MDL of each element.

An error in sample preparation resulted in a Se-Fe-Cu doped sample becoming contaminated with a high amount of Aluminum. This sample was prepared by pouring the desired standard solutions directly onto a piece of filter paper which was on a sheet of aluminum foil. The sample was then left to soak overnight on the foil, as the liquid naturally evaporated. This allowed the nitric acid present within the standard solutions to chemically react with the aluminum present on the foil, which resulted in a large amount of aluminum being deposited onto this

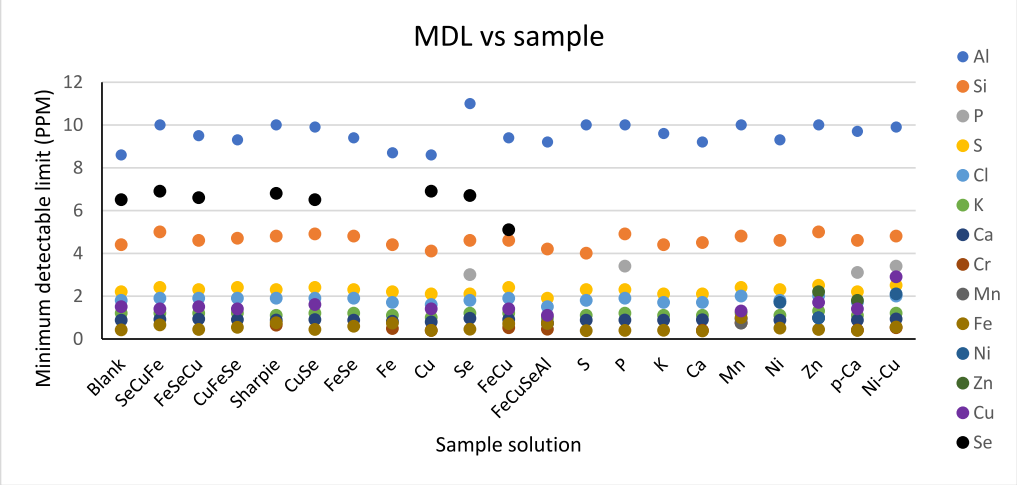

Fig. 5. MDL values obtained for each element detected in every prepared sample.

sample. While all other samples had an average concentration of 187 ppm, the contamination of this sample was evident by the increased concentration of 4663 ppm. In Table 3, this sample has been labelled as Se-Fe-Cu-Al to indicate the aluminum contamination. MDLs are slightly elevated in the Ni-Cu sample compared to those obtained in single element samples. This is not entirely unexpected, as the high overlap between the nickel K_β and copper K_α x-rays has been shown to reduce detection limits. Ryan et al. discusses this in detail, and others have attempted to minimize the effects of x-ray overlap by employing wavelength dispersive x-ray spectrometers [29,30]. However, due to GeoPIXE using the statistics from both the K_α/K_β peaks it's unlikely that the increased detection limits are due to peak overlap and are more than likely due to matrix effects. Fig. 4 shows the x-ray spectrum obtained for the Ni-Cu combination doped sample analyzed by the GeoPIXE software package. Aside from the Ni-Cu sample however, all other combination doped samples yielded MDL that did not abnormally deviate significantly from previous data runs.

Both the filter paper matrix itself and the standard elemental solutions used contain trace amounts of various elements that were not originally intended for study. Since these trace elements were still present however, the MDL for these different elements were able to be obtained utilizing the GeoPIXE software. Table 4 lists the MDL in PPM for elements that were not originally intended for study. Finally, Fig. 5 displays the MDL for each element in all the samples that were evaluated. It is thought that the consistent presence of aluminum contamination was due to the samples being rested on aluminum foil after preparation, while other elements such as Silicon and Chlorine are naturally present in the filter paper matrix. The source of contamination for Chromium remains unknown, though it is thought that this may have been a result of environmental contamination in the laboratory.

4. Conclusions

The data obtained yields consistent MDL for each element of interest that was studied. In an analogue biological matrix consisting primarily of cellulose, the MDL varies depending on the element of interest but was consistently found to be on the order of a few PPM. An analytical determination of both concentrations and detection limits is even possible with elements that have high overlap in x-ray energies, though the MDL may be elevated in this case. Aside from samples with elemental compositions containing overlapping x-ray energies, detection limits are independent of concentrations of elements present. Additionally, the MDL of elements in filter paper was found to be independent of the order in which samples were deposited onto it, allowing for the easy determination of detection limits for multiple elements. Several studies have investigated both the concentration and the detection limits of various elements in both NIST verified standards and in actual tissue samples [31]. Previous PIXE analysis of human brain tissue has found that detection limits for elements with atomic numbers $Z \geq 20$ is frequently on the order of 1 ppm [32]. A comparative study between EXRF, TXRF, synchrotron radiation and PIXE on several human tissue types is given by and again finds similar results [33]. Unfortunately both studies demonstrated detection limits for lighter elements of $Z \geq 20$ above 10 ppm which does not agree well with the results found here. However, this is most likely due to the difference in the experimental setup used in both experiments, mainly due to the use of outdated SiLi detectors, and their low detection efficiencies for light elements. This makes an inter-comparison of these results to other studies mostly qualitative, so further investigation is needed to determine the accuracy of these detection limits compared to actual biological samples. Furthermore, if lower detection limits are desirable for a particular element of interest, optimizing beam parameters is a proven way of improving detection limits. By carefully selecting beam energies to maximize the x-ray cross section of an element of interest, as well as maximizing the effective solid angle of the x-ray detector used are both known methods to obtain lower detection limits. Additionally, higher charge collection will result in better statistics, allowing for weaker peaks to possibly rise above background levels. A discussion on improving PIXE detection limits specifically for biological applications is given by [34]. Future experiments interested in the MDL of different elements should vary the probing beam energy along with the matrix composition used.

Author contributions

C.T.B., T.A.B, B. R. and G.A.G conceived and supervised this work and wrote the manuscript. C. N., D.K.S. participated in the PIXE experimentation and analysis on the samples, and revision of the manuscript. G.A.G., B. R. provided the funding, supervision, and writing of the manuscript.

Data availability

All the data generated or analyzed during this study are included in the published article. Any data related to this study can be provided with reasonable request.

Declaration of competing interest

The authors declare that they have no known competing financial

interests or personal relationships that could have appeared to influence the work reported in this paper.

Acknowledgements

We acknowledge partial support from NIH grant # NIH-R01DK109382 and NSF grant # 2210722.

References

[1] C. Grochowski, et al., Analysis of trace elements in human brain: its aim, methods, and concentration levels, Front. Chem., 7 (2019), [Online]. Available: https://www.frontiersin.org/articles/10.3389/fchem.2019.00115.
[2] R. Squitti, Copper dysfunction in Alzheimer's disease: from meta-analysis of biochemical studies to new insight into genetics, J. Trace Elem. Med Biol. 26 (2–3) (Jun. 2012) 93–96, https://doi.org/10.1016/J.JTEMB.2012.04.012.
[3] B.D. Corbin, et al., Metal chelation and inhibition of bacterial growth in tissue abscesses, Science (1979) 319 (5865) (Feb. 2008) 962–965, https://doi.org/10.1126/SCIENCE.1152449/SUPPL_FILE/CORBIN.SOM.PDF.
[4] R.W. Hutchinson, et al., Imaging and spatial distribution of β-amyloid peptide and metal ions in Alzheimer's plaques by laser ablation–inductively coupled plasma–mass spectrometry, Anal. Biochem. 346 (2) (Nov. 2005) 225–233, https://doi.org/10.1016/J.AB.2005.08.024.
[5] C.G. Fraga, Relevance, essentiality and toxicity of trace elements in human health, Mol. Aspects Med. 26 (4–5) (Aug. 2005) 235–244, https://doi.org/10.1016/J.MAM.2005.07.013.
[6] J.R. Nuttall, P.I. Oteiza, Zinc and the aging brain, Genes Nutr.. 9 (1) (2014), https://doi.org/10.1007/s12263-013-0379-x.
[7] M.P. Cuajungco, G.J. Lees, Zinc metabolism in the brain: relevance to human neurodegenerative disorders, Neurobiol. Dis. 4 (3–4) (1997) 137–169, https://doi.org/10.1006/nbdi.1997.0163.
[8] K. Vogel-Mikuš, P. Pongrac, P. Pelicon, Micro-PIXE elemental mapping for ionome studies of crop plants, 24(03n04) (Nov. 2015), 217–233. doi: 10.1142/S0129083514400142.
[9] D.A. Cataldo, R.E. Wildung, Soil and plant factors influencing the accumulation of heavy metals by plants, Environ.. Health Perspect. 27 (1978) 149–159, https://doi.org/10.1289/EHP.7827149.
[10] F.H. Nielsen, Ultratrace elements in nutrition, Annu. Rev. Nutr. 4 (1) (Jul. 1984) 21–41, https://doi.org/10.1146/ANNUREV.NU.04.070184.000321.
[11] S. Takahashi, I. Takahashi, H. Sato, Y. Kubota, S. Yoshida, Y. Muramatsu, Age-related changes in the concentrations of major and trace elements in the brain of rats and mice, Biol.. Trace Elem. Res. 80 (2) (2001) 145–158, https://doi.org/10.1385/BTER:80:2:145.
[12] C.G. Ryan, PIXE and the nuclear microprobe: Tools for quantitative imaging of complex natural materials, Nucl Instrum Methods Phys Res B 269 (20) (Oct. 2011) 2151–2162, https://doi.org/10.1016/J.NIMB.2011.02.046.
[13] S.A.E. Johansson, T.B. Johansson, Analytical application of particle induced X-ray emission, Nucl. Inst. Methods 137 (3) (1976) 473–516, https://doi.org/10.1016/0029-554X(76)90470-5.
[14] S.A.E. Johansson, J.L. Campbell, K.G. Malmqvist, Particle-induced X-ray emission spectrometry (PIXE), p. 451, 1995, Accessed: Jan. 23, 2024. [Online]. Available: https://www.wiley.com/en-us/Particle+Induced+X+Ray+Emission+Spectrometry+%28PIXE%29-p-9780471589440.
[15] T.A. Byers, J.E. Manuel, A.G. Ponette-Gonzalez, T.E. Gill, G.A. Glass, Analysis of rain-deposited dust on polysulfone membranes using proton-induced X-ray emission spectroscopy, Microchem. J. 192 (Sep. 2023) 108928, https://doi.org/10.1016/J.MICROC.2023.108928.
[16] S. Juma Mulware, B. Rout, T. Reinert, N. Dasgupta-Schubert, "Quantitative Analysis of the Effect of Carbon Nanotubes on the Iron (Fe) [Online]. Available: Uptake by Corn Roots" (2018) http://www.aascit.org/journal/ijabe.
[17] I.E. Kieft, D.N. Jamieson, B. Rout, R. Szymanski, A.S. Jamieson, PIXE cluster analysis of ancient ceramics from North Syria, Nucl Instrum Methods Phys Res B 190 (1–4) (May 2002) 492–496, https://doi.org/10.1016/S0168-583X(01)01284-8.
[18] K. Ishii, S. Morita, Continuous backgrounds in pixe, vol. 01, no. 01, pp. 1–29, Jan. 2012, doi: 10.1142/S0129083590000025.
[19] M. Kavčič, Improved detection limits in PIXE analysis employing wavelength dispersive X-ray spectroscopy, Nucl Instrum Methods Phys Res B 268 (22) (Nov. 2010) 3438–3442, https://doi.org/10.1016/J.NIMB.2010.09.003.
[20] J.E. Manuel, et al., Fish gelatin thin film standards for biological application of PIXE, Nucl Instrum Methods Phys Res B 332 (2014) 37–41, https://doi.org/10.1016/j.nimb.2014.02.025.
[21] "Fisherbrand Qualitative Grade Plain Filter Paper Circles - P8 Grade Circles; | Fisher Scientific." Accessed: Jan. 21, 2024. [Online]. Available: https://www.fishersci.com/shop/products/qualitative-grade-plain-filter-paper-circles-p8-grade/09795C#?keyword=.
[22] B. Rout, et al., An overview of the facilities, activities, and developments at the University of North Texas Ion Beam Modification and Analysis Laboratory (IBMAL), AIP Conf. Proc. 1544 (1) (Jul. 2013) 11–18, https://doi.org/10.1063/1.4813454.
[23] B. Rout et al., "Ion Beam Materials Analysis and Modifications At keV to MeV Energies at the University of North Texas," 2013 International Conference on Applications of Nuclear Techniques, June 23-29, 2013. Crete, Greece, vol. 27, p. 1460147, Feb. 2014, doi: 10.1142/S2010194514601471.
[24] Wickramaarachchige J Lakshantha, Mangal S Dhoubhadel, Tilo Reinert, Floyd D McDaniel, Bibhudutta Rout, "Investigation of various phases of Fe–Si structures formed in Si by low energy Fe ion implantation," Nucl Instrum Methods Phys Res B, vol. 365, Part A, pp. 114-119, 2015, https://doi.org/10.1016/j.nimb.2015.07.037.
[25] "Patented C-Series Low Energy X-Ray Windows – Amptek – X-Ray Detectors and Electronics." Accessed: Jan. 31, 2024. [Online]. Available: https://www.amptek.com/products/x-ray-detectors/fastsdd-x-ray-detectors-for-xrf-eds/c-series-low-energy-x-ray-windows.
[26] C.G. Ryan, D.R. Cousens, S.H. Sie, W.L. Griffin, G.F. Suter, E. Clayton, Quantitative pixe microanalysis of geological matemal using the CSIRO proton microprobe, Nucl Instrum Methods Phys Res B 47 (1) (Mar. 1990) 55–71, https://doi.org/10.1016/0168-583X(90)90047-X.
[27] C.G. Ryan, Quantitative trace element imaging using PIXE and the nuclear microprobe, Int. J. Imaging Syst. Technol. 11 (4) (Jan. 2000) 219–230, https://doi.org/10.1002/IMA.1007.
[28] C.G. Ryan, E. Clayton, W.L. Griffin, S.H. Sie, D.R. Cousens, SNIP, a statistics-sensitive background treatment for the quantitative analysis of PIXE spectra in geoscience applications, Nucl Instrum Methods Phys Res B 34 (3) (Sep. 1988) 396–402, https://doi.org/10.1016/0168-583X(88)90063-8.
[29] M. Kavčič, M. Žitnik, K. Bučar, J. Szlachetko, Application of wavelength dispersive X-ray spectroscopy to improve detection limits in X-ray analysis, X-Ray Spectrom. 40 (1) (Jan. 2011) 2–6, https://doi.org/10.1002/XRS.1291.
[30] C.G. Ryan, E. Van Achterbergh, D.N. Jamieson, C.L. Churms, Overlap corrected on-line PIXE imaging using the proton microprobe, Nucl Instrum Methods Phys Res B 109–110 (Apr. 1996) 154–160, https://doi.org/10.1016/0168-583X(95)00898-5.
[31] M. Ali, PIXE and RIXRF comparison for applications to biological sample analysis, Nuclear Instruments & Methods in Physics Research Section B-Beam Interactions with Materials and Atoms 222 (3–4) (Aug. 2004) 567–576, https://doi.org/10.1016/J.NIMB.2004.02.033.
[32] M. Boruchowska, M. Lankosz, D. Adamek, A. Korman, PIXE analysis of human brain tissue, X-Ray Spectrom. 30 (3) (May 2001) 174–179, https://doi.org/10.1002/XRS.484.
[33] M.L. Carvalho, T. Magalhães, M. Becker, A. von Bohlen, Trace elements in human cancerous and healthy tissues: A comparative study by EDXRF, TXRF, synchrotron radiation and PIXE, Spectrochim Acta Part B at Spectrosc 62 (9) (Sep. 2007) 1004–1011, https://doi.org/10.1016/J.SAB.2007.03.030.
[34] J.L. Campbell, S.B. Russell, S. Faiq, C.W. Schulte, R.W. Ollerhead, R.R. Gingerich, Optimization of PIXE sensitivity for biomedical applications, Nucl. Inst. Methods 181 (1–3) (Mar. 1981) 285–292, https://doi.org/10.1016/0029-554X(81)90622-4.